Advanced Simulation Technologies for Next-Generation Transmission Fibers

Zoltán Várallyay[*1], *Kazunori Mukasa*[*2], *Tamás Mihálffy*[*1], *Sándor Bilicz*[*3],
Bence Németh[*1], *Péter Szelestey*[*1], *Béla Csengeri*[*1],
Zsolt Puskás[*1], *Gábor Varga*[*1,*3], *Yoshihiro Arashitani*[*2]

ABSTRACT The simulation for optical characteristics of optical fibers is an important key technology in optical fiber research, and development and manufacturing. Among them, though the micro-bending loss and Rayleigh scattering loss are extremely important characteristics, it is difficult to predict these characteristics with simulations due to the complex phenomena. In these respects, for the micro-bending loss, we developed a new simulation method which combines the mechanical effects and the optical effects by using the coupled mode theory, and regarding Rayleigh scattering, we also developed a method for finding changes in the glass-membered ring structure distribution by using molecular dynamic (MD) simulations. And we have successfully studied various characteristics to be reported.

1. INTRODUCTION

Large-capacity communication using optical fibers has become one of the indispensable foundations in our daily lives. Due to the spread of COVID-19 and growing demands for exhaust gas control, the demand for the optical communication tends to increase further. And even the higher capacity communication by improving the characteristics of communication fiber cables is strongly required.

One solution is to increase the number of the optical fibers in the optical fiber cables. However, outside diameters of the cables are required to be maintained at the same sizes as before, then the optical fibers are required to have smaller diameters than before in order to contribute to higher density.[1), 2)] However, this modification of the optical fibers shall be carefully approached since smaller sizes will suffer larger deformation under the influence of deforming mechanical effects and consequently larger loss of the transmission will be experienced. This is the micro-bending loss, which is very important as an index to the change in characteristics after cable manufacturing. In order to reduce the micro-bending loss, optimization of the optical fiber structure is important.[2)-5)] But, the characteristics prediction by simulation was difficult as submicron order fine and random deformation in the optical fiber has to be dealt with.

One of the other solutions is to reduce the transmission loss of the optical fiber itself. Transmission loss is largely dominated by the glass structure, and the technology to determine how the glass structure changes depending on the temperature, the pressure, and the dopant material by simulation becomes very important[6)]. Also, the micro-changes on molecular level is necessary to be dealt with, and it was necessary to build very advanced technology as well.

The simulation of the micro-bending loss requires to take into account not only the optical effects (solving the Helmholtz Eigen value equation) but also the mechanical properties of the glass and the coatings. For the description of the optical characteristics, the Coupled Mode Theory (CMT)[7)] is used which evaluates the coupling of the propagating core modes to radiation cladding modes due to micro-deformations of the fiber glass. On the other hand, despite the importance of the mechanical investigations, only few investigations have been reported so far[8), 9)]. For discrete deformations in space where the extent of the distortion is smaller than their average discrete distances, Olshansky came up with the expression of the power spectrum of the deformation by a correlation function using a power form with a problem specific adjustable parameter[10)]. This kind of correlation function to calculate the micro-bending loss is recently used to evaluate the micro-bending loss properties of trench type optical fibers[11)] having more complicated structures than simple step-index type optical fibers and we also proceeded with studies using this correlation function in order to evaluate the micro-bending loss characteristics of optical fibers with complex profiles such as the trench type optical fibers and confirmed a good relation with the measured values[3)-5)].

[*1] Simulation Group, FETI Ltd.
[*2] Telecommunications & Energy Laboratories, R&D Division, Furukawa Electric Co., Ltd.
[*3] Budapest University of Technology and Economics

On the other hand, Rayleigh scattering loss in a current optimized silica based optical fiber has the largest contribution to the total loss of the waveguide at around the telecommunication wavelengths. Rayleigh scattering losses are mostly originating from the glass-membered ring structure distribution in the spatial range of 10 Å[12] if dopant concentrations in the glass are small enough. In order to reduce the scattering loss of the glass, one may have three options.

1) Optimize the optical fiber cooling condition including the annealing treatment in the fiber drawing[13)-16)].
2) Apply some pressure on the melted state of the glass preform[17), 18)] .
3) Add some dopants such as large ions to the glass that can modify the network structure of silica within the range not to cause the large fluctuation in the ion concentration[19)].

However, experimental optimization of the conditions would require a lot of efforts. Instead, MD simulation can be used to study the micro changes in the glass structure under different processing conditions. So far, most of the glass structure studies have been carried out by using the two-body interaction potentials[13), 14)]. In addition to these, in order to investigate the changes in glass structures caused by different process conditions and dopants with higher accuracy, we also investigated the three-body interaction potentials and confirmed interesting results.

For this time, we conducted a simulation study with the following two aspects, and are reporting here the details.

1) Decrease the sensitivity of the fiber against the micro-bending loss which is an important factor showing the increase in the loss due to the fine deformations from the cabling process.
2) Decrease Rayleigh scattering loss, which is largely dominated by the uniformity of glass structure, in a drawing process and by the dopant materials.

2. MICRO-BENDING LOSS SIMULATIONS

2.1 Theory

Micro-bending loss based on the CMT is calculated, as shown in Equation (1), by the multiplication of the coupling coefficient C_{1s}^2 (between the LP_{01} core transmission mode and the LP_{1s} type radiation modes) and the power spectrum of the deformation function $\Phi(\Delta\beta_{1s})$:

$$2\alpha_m = \sum_{s=1}^{\infty} C_{1s}^2\, \Phi(\Delta\beta_{1s}) \tag{1}$$

where $\Delta\beta_{1s} = \beta_{01} - \beta_{1s}$ is the difference in propagation constant between the LP_{01} core mode and the LP_{1s} radiation mode, where s=1, 2, …, ∞ . Here we can do the summation for a finite number of radiation modes due to the nature of $\Phi(\Delta\beta_{1s})$ that is a decaying function resulting in negligible small contribution from large s values. To evaluate the coupling coefficient, one needs a mode solver to obtain the electric field distributions of the necessary modes. By using the electric field distribution, the coupling coefficient can be evaluated by the following Equation (2).

$$C_{1s}^2 = \frac{k^2}{2} \frac{\left(\int_0^{\infty} \frac{\partial n_0}{\partial r} E_{01} E_{1s}\, rdr\right)^2}{\int_0^{\infty} E_{01}^2 rdr \int_0^{\infty} E_{1s}^2 rdr} \tag{2}$$

Where E_{01} is the electric field distribution of LP_{01} and E_{1s} is the field distribution of LP_{1s} modes, k is the wavenumber and n_0 is the initial refractive index profile of the fiber without any deformation. The normalized power spectrum for the deformation distribution given by the $f(z)$ function is given by the following Equation (3).

$$\Phi(\Delta\beta_{1s}) = \frac{1}{2L}\left|\int_{-L}^{L} f(z)\exp(-i\Delta\beta_{1s}z)dz\right|^2 \tag{3}$$

where L is the length of the deformation centered around zero, and z is the axial coordinate. Method to choose a deformation function that has a power spectrum in the form of $1/\Delta\beta_{1s}^{2p}$ was introduced by Olshansky[10] where p=1.1 was obtained by measuring a coiled fiber on a fiber drum[8]. However, there is a question what value we can get for p in the sandpaper test with a higher surface roughness than that in REFERENCE 8). In response to this question, we created a list that can simulate experimental conditions with high accuracy, and set up an environment that can be optimized without experimentation.

Other shape of the normalized power spectrum of the other form of the deformation function at the spatial frequency $\Delta\beta_{1s}$ can be found by examining the mechanical deformation of the fiber on sandpaper particles. We compared our micro-bending loss measurement data with the calculated results using different shape of the power spectrum of the deformations, and we fit the p exponential factor with the experimental results. We also introduced a new type of $\Phi(\Delta\beta_{1s})$ formula based on the mechanical simulations and compared the results with the approximate values introduced in REFERENCES 10) and 11).

Regarding mechanical fluctuations, we have analyzed the optical fiber as it is deformed by a particle using the finite element analysis. The model contains a piece of fiber fragment, and its end facets are disabled to move in the z and y directions, allowed only up and down movement (x-direction, See Figure 1). One end of the fiber is touching the particle and the other end is loaded by a force that has a magnitude comparable to the tension used during fiber coiling in the experiments. The obtained displacement function with a fiber length of 1 mm is shown in Figure 1 where displacement of the core resembles to a Gaussian profile. If we assume that the deformation function has a Gaussian shape, we can write that function in the following form.

$$f(z) = Ae^{-\frac{z^2}{2b^2}} \tag{4}$$

where A and b are positive, real numbers. Similarly, a deformation function in the form of $A \cdot z \cdot e^{-z^2/(2b^2)}$ can be defined but as we show below this does not add to the accuracy of the micro-bending loss modeling related

to the sandpaper test. By using Equation (3), one can calculate the power spectrum of the deformation given by Equation (4) and obtaining the following Equation (5).

$$\Phi(\Delta\beta_{1s}) = (Ab)^2 e^{-b^2\Delta\beta_{1s}^2} \tag{5}$$

where A is practically the amplitude of the deformation which is proportional to the diameter of the fiber glass and the thickness of the coatings. Therefore, one can write the micro-bending loss in the following form using Equations (1) and (5) and the assumption for the amplitude (A) suggested in RFERENCES 3),4) (secondary coating has small contribution and is omitted now).

$$2\alpha_m = \overbrace{a^2 \cdot e^{-\frac{2d_g}{\tau_g}} e^{-\frac{2t_p}{\tau_p}}}^{\text{Mechanical effect}} \cdot \underbrace{b^2 \sum_{s=1}^{N} C_{1s}^2 \cdot e^{-b^2\Delta\beta_{1s}^2}}_{\text{Optical effect } (Y)} \tag{6}$$

Where d_g is the diameter of the fiber glass, t_p is the thickness of the primary coating and a, τ_g, τ_p are parameters characteristic to the experiment. The first three terms are related to the magnitude of the deformation called mechanical characteristics, and the term added to them is related to the mode overlap and the propagation constant difference, thus the optical properties.

For the mechanical simulation, in consideration of the stiffness of the glass and the coatings, a 125 μm standard glass diameter and a standard coating thicknesses with 250 μm outer diameter were used. The order of the deformation magnitude obtained in Figure 1 is sub-micrometer, which is in good agreement with the values obtained in recent experiments on the shape and the magnitude of micro-deformations using a multi-core fiber[9].

2.2 Results in Micro-bending Loss Simulations

We used the description obtained in Equation (6) to calculate the micro-bending loss for each experimentally investigated optical fiber designs by applying three different deformation functions(Table 1). For the calculation we used $1/\Delta\beta_{1s}^{2p}$, that is the functional form introduced by Olshansky[10] with $p = 0$, 1, 2, and $e^{-b^2\Delta\beta_{1s}^{2p}}$, that is obtained in Equation (5) assuming the Gaussian deformation of the fiber and an additional exponential factor p similar to Olshansky's formula. As it is shown in Table 1, we have also calculated using $\Delta\beta_{1s}^{2p} e^{-b^2\Delta\beta_{1s}^{2p}}$ power spectrum function but this did not improve the micro-bending model giving the same regression parameter as for the Gaussian deformation.

The loss calculation is inserted into a constrained optimization algorithm with minimum and maximum boundaries and changed the parameters until the best fit is obtained reconciling with the experimental results. The two different power spectra of the deformations show the different simulation results as shown in Figure 2 and the fitted lines have different slopes on the graph. The correlation between the two different calculation methods and the measurements are good for both models but slightly better for the Gaussian approximation obtained by Equation (5). R^2 regression parameter is 0.934 for the first case and 0.951 for the Gaussian form as shown in Table 1 and 0.95 for the more complicated, combined Gaussian and power formula. The p parameter in the $1/\Delta\beta_{1s}^{2p}$ formula is obtained to be 2.2387 for the sandpaper test that is close to 2 as mentioned in REFERENCES 8) and as a contrast to 1.1 in REFERENCES 3) where the surface roughness was less than in our experiments with the fibers coiled on sandpaper.

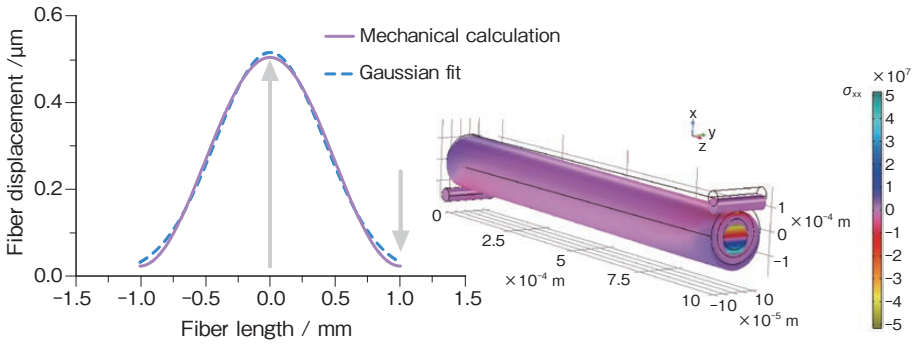

Figure 1 The model to calculate the mechanical deformation of a piece of fiber including primary and secondary coatings, and the obtained displacement function along with a fitted Gaussian profile.

Table 1 Different deformation functions, power spectrum of the deformations, obtained parameters and the accuracy of the regression (R^2). A amplitude parameter contains a, τ_g, τ_p as it is written in Equations (4), (5) and (6).

$f(z)$	$\Phi(\Delta\beta_{1s})$	a	τ_g	τ_p	b	p	R^2
$A\cdot\lvert z\rvert$	$A\ \Delta\beta_{1s}^{-2p}$	10^5	12.8	9.8	–	2.2387	0.934
$A\cdot e^{-z^2/(2b^2)}$	$A^2b^2e^{-b^2\Delta\beta_{1s}^{2p}}$	10^3	25.4	19.5	3.02	0.2582	0.951
$A\cdot z\cdot e^{-z^2/(2b^2)}$	$A^2\cdot b^6\cdot\Delta\beta_{1s}^2\cdot e^{-b^2\Delta\beta_{1s}^{2p}}$	$10^5/6$	25.4	19.5	4.04	0.2043	0.950

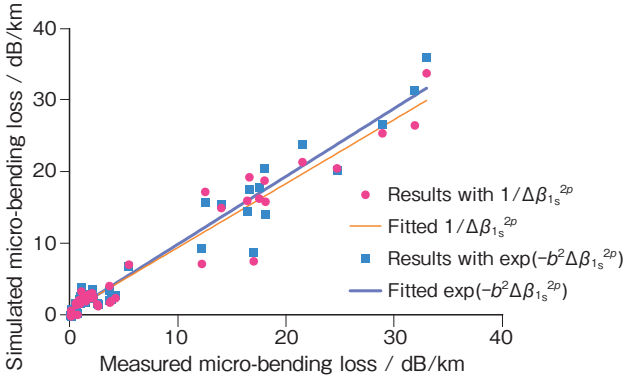

Figure 2 The measured and simulated micro-bending loss using two different power spectrum functions at 1550 nm.

The obtained parameter set that provides the best fit with the combined micro- and macro-bending effects are the following

$$p = 2.67,\ A=10^5,$$
$$\tau_1 = 12.8\ \mu m,\ \tau_2 = 9.8\ \mu m,\ \tau_3 = 29.6\ \mu m \qquad (7)$$

These parameters and the CMT model are used to calculate the micro-bending loss as a function of the wavelength shown in Figure 3. The calculated results are compared with the measurement results of a step-index waveguide and a trench assisted fiber. Values predicted by the calculations show good agreement with the measured values. We use therefore this model in the followings to evaluate the micro-bending loss of different fiber designs.

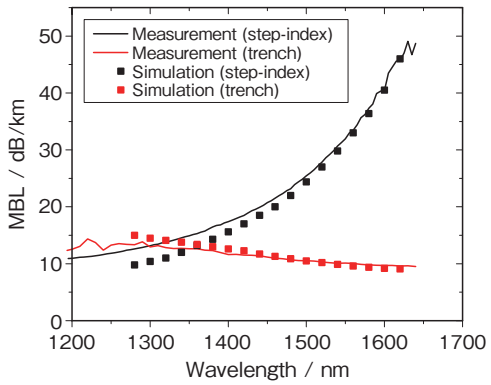

Figure 3 Calculated and measured wavelength dependency of MBL in a step-index fiber with 68 µm and a trench assisted fiber with 80 µm glass diameter.

We also tested the coating behavior based on Equation (6), in such a manner that the term for the secondary coating is similar to the one of the primary coating, and we compared the effect of coating thicknesses in the simulations with the measurements. To do this, the measured and calculated results on the micro-bending loss are divided by the calculated optical factor (*Y*) and that part of the mechanical factor that does not contain the investigated parameter. For example, if we investigated the effect of glass diameter, we divide the measured and calculated α_m by $Y \cdot e^{-2t_p/\tau_2} \cdot e^{-2t_s/\tau_3}$. This way, according to Equation (6) we obtain $a^2 e^{-2d_g/\tau_1}$ which is a pure exponential function for the calculations and those operations should yield a similar behavior on the measured data as well. This test is visualized in Figure 4 where the measured data shows similar exponential decay with increased glass diameter (Figure 4 (a)) and the primary coating thickness (Figure 4 (b)) as the calculation results. This indicates that the glass diameter and the primary coating thickness parameters are essential properties from the micro-bending loss point of view. According to Figure 4 (c), the secondary coating does not show such a clear trend for the measurements than the one that is obtained from the theoretical investigations. The shallow slope of the nearly linear function of Figure 4 (c) is still decreasing with increased secondary coating thicknesses but the measured micro-bending loss has an even weaker correlation to the secondary coating. We can state that in general, Equation (3) is a good approximation to describe the mechanical properties with the properly fitted parameter set. And also, the secondary coating does not play an important role in the micro-bending loss reduction.

As an example, we investigated a simple step-index fiber design consisting of a core and a cladding region. This investigation can establish the relation between the effective core area and the fiber parameters. The results with different core sizes ($2a$) and the core-cladding relative index differences (Δ)of the step-index design are shown in Figure 5. The parameter ranges used in the calculations are the following: Δ_1 = 0.32, 0.33, …, 0.42% and $2{\cdot}a$ = 8, 9, …, 13 µm. In most cases for the relative core index difference, one can find an optimum core size that corresponds to a certain core relative index difference that

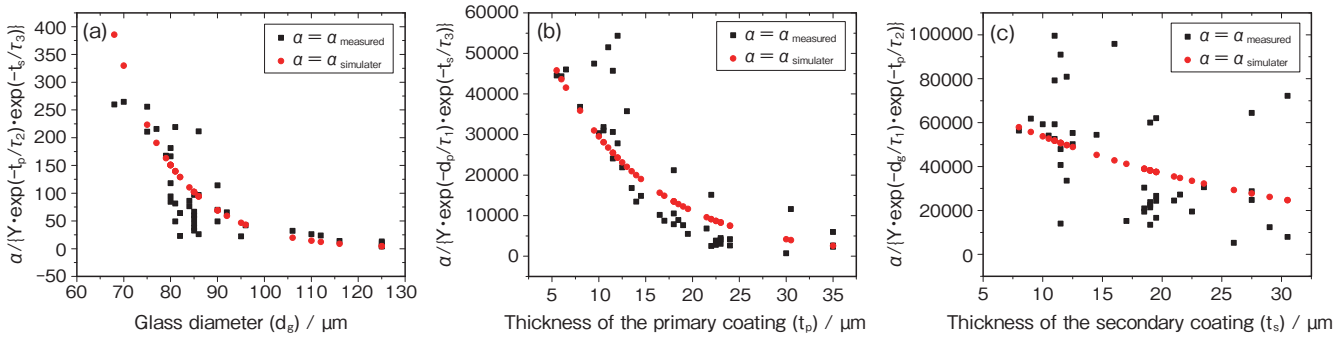

Figure 4 The measured and calculated micro-bending loss divided by the optical factor *Y* and the exponential mechanical factors for the disjoint fiber properties as functions of (a) glass diameter, (b) primary coating thickness and (c) secondary coating thickness.

provides a minimum micro-bending loss. For example, for Δ_1 = 0.32%, the optimum value is between $2a$ = 9 μm and $2a$ = 10 μm. Smaller than the optimum core size will enhance the coupling of the fundamental core mode to radiation cladding modes. At a fix core size, the smaller the relative core index difference, the larger the effective core area as well as the micro-bending loss. More complex structures can be investigated and analyzed with our model. The model can be used in conjunction with other models that can calculate other fiber parameters (dispersion, cut-off wavelength, mode-field diameter, etc.), and it becomes possible to study and analyze in consideration of various characteristics trade-off.

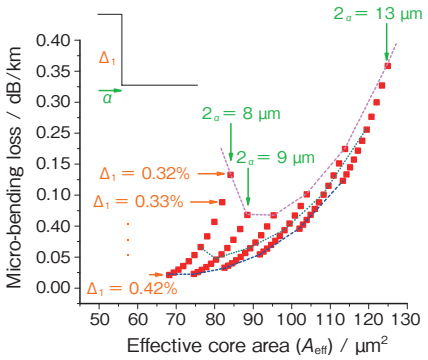

Figure 5 The micro-bending loss as a function of an effective core area in a step-index fiber, by changing two fiber parameters: the relative index difference of the core (Δ_1) and the core radius (a).

3. RESULTS IN GLASS SIMULATIONS

In MD simulations, we cool down the amorphous SiO_2 structure with few thousands of atoms from the melting (furnace) temperature to room temperature as it is happening during the fiber drawing process. We changed and investigated the effect of cooling rate; we introduced different cooling patterns and we checked the effect of the initial temperature (furnace temperature) as well. The effect of pressure during the drawing process was also calculated applying different magnitude of pressure on the melted state of the glass at the beginning of the drawing process. For the simulation of the cooling process, we used the Vashishta potential[20] with N=number of particles, V=volume, T=absolute temperature (NVT) ensemble and for the pressure effects the Tersoff potential[21] is applied because that can capture the pressure dependent effects with an N=number of particles, P=pressure, T=absolute temperature (NPT) ensemble which is more reliable compared to the Vashishta potential because it does not handle the melted state of the glass well in atmospheric pressure with the original parametrization. For dopants we calculated with different concentration of Cl and F-doping in SiO_2 glass using the Ohta-Hamaguchi potential[22]. All these investigations showed that these effects may have significant influence on glass homogeneity at a microscopic level.

Our model contained 3375 randomly placed Si and O atoms in a 37 Å rectangular box at 1000˚C initial temperature. We noted that the Tersoff potential needs significantly higher temperature range to cause the melting of the glass than what is happening in the reality; this fact is known from the literature[23] but pressure related calculations remain close to the range of natural behavior, for instance, system does not goes apart on close to atmospheric pressure as it does with the Vashishta potential with NPT ensemble.

We expect a glass transition temperature between 1300˚C and 1800˚C for silica but using the Tersoff potential in an MD simulation this happens at around 2500˚C. This is due to the parameter settings of the potential. We used its original parametrization as described in REFRENCES 21). This is a recognized problem with MD simulations and could be overcome with the re-parametrization of the force-field. With the original parametrization however, the annealing process is set to heat up the system to 5000˚C and cool down to room temperature in case of pressure dependent calculations. The cooling is approximated by a linear function as a function of time in our models. Figure 6 entirely corresponds to calculations with the Vashishta potential. Figure 6 (a) shows the glass-membered ring structure distribution obtained as an effect of different cooling rates using NVT ensemble. The clear trend with the increasing glass homogeneity can be seen with the decreasing cooling rate that is indicated also with the fitted Gamma functions. That may be also in general interesting in what will happen if we cool down

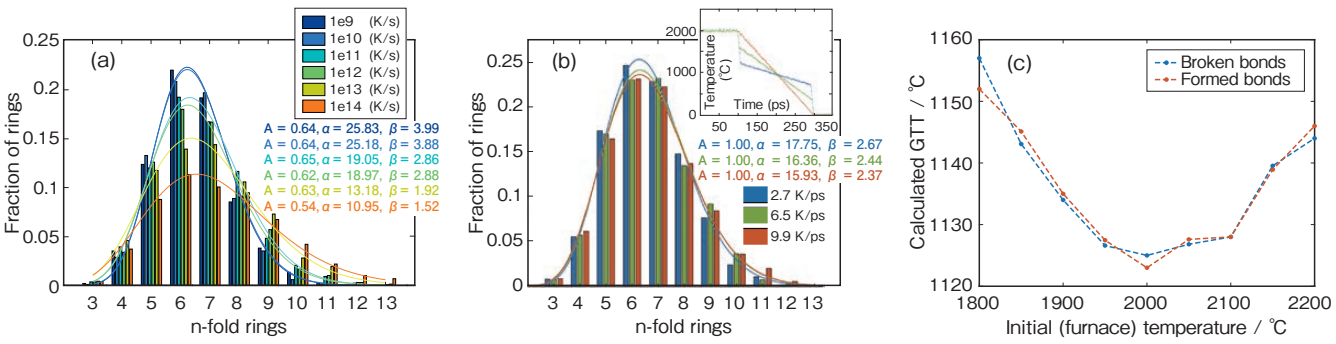

Figure 6 (a) The glass-membered ring structure distribution and Gamma function fitted curves for different cooling rates with constant temperature change along the fiber. (b) The glass-membered ring structure distribution and Gamma function fitted curves when the cooling rate is changed near the GTT of the glass. (c) The relations between the GTT of the glass and the initial temperature.

the fiber with varying cooling rate between the output window of the furnace (~2000℃) and the coiling of the fiber (~room temperature). What will happen if we slow down the cooling just around the glass transition temperature (GTT) of the glass (at around 1250℃ in this example)? Corresponding cooling patterns are shown in the inset of Figure 6 (b). The idea is that we cool down the fiber with the same average speed or with the same time in order to apply the coating after the fiber reaches the required temperature to be able to receive the coating, but the cooling rate is slow around the GTT of the glass. One may set some additional furnaces to heat up the environment of the fiber and slow down the cooling at that segment. Figure 6 (b) shows the glass-membered ring structure of the corresponding structures at the different cooling around the GTT of the glass. The constant cooling (red curve in Figure 6 (b) and red bars) has the most diverse glass-membered ring structure distribution meaning that statistically the large number-fold glass-membered ring structures and the three membered ring and the four membered ring structures are in the highest number in this structure. The effect of the initial temperature or the furnace temperature on the final structure can be interesting too. That is shown in Figure 6 (c). We calculated the same cooling process as before, but the cooling rate is chosen at a constant 10^{12} K/s for each simulation, and the initial temperature is changing between 1800℃ and 2200℃. A minimum in GTT of the glass was found at around 2000℃.

We calculate and investigate also the impact of applying pressure on the melted state of the fiber glass that can be achieved, for instance, by introducing a pressure chamber below the furnace. The obtained changes in density at different pressures are shown in Figure 7 (a) using 10^{12} and 10^{13} K/s cooling rates. The presented results are averages of five different calculation sets with five different random seeds for initial speed vectors and directions of the atoms at the beginning of the MD simulations. These curves show that the final density of the glass depends on the pressure, but we have to note that the error of the calculation is acceptable only at above 1MPa pressure. At low pressures, the calculated pressure values from MD are noisy. Regarding the pressure dependence of the two calculated cases, we can see the change in the density of the glass above an applied pressure of 10 MPa value. The density of the glass here is 2.256 g/cm^3 while the density is 2.254 g/cm^3 at 1 MPa for 10^{12} K/s cooling rate.

The obtained glass-membered ring structure distribution can be seen in Figure 7 (b). The applied pressure doesn't significantly affect the number of the three membered ring or the four membered ring in the structure. The difference between differently pressurized melted glasses appears in the large number of the glass-membered ring structures such as the eight membered ring, the nine membered ring, the ten membered ring, etc. This fact indicates that the applied pressure suppresses the voids in the silica structure which is also stated in REFERENCES 18).

For doped glass simulations (Cl, F), we have tested by implementing the Ohta-Hamaguchi potential which potential is originally developed for etching purposes for Silica[22] that can describe interactions between Si, O and halogen atoms with two- and three-body interactions. We use a system with 3375 Si and O atoms to test the effect of different Cl doping with 10^{13} K/s cooling rate. This potential is computationally intensive therefore we stick first with the 10^{13} K/s cooling, and we will carry out computations with 10^{12} K/s later. Figure 8 (a) shows a small portion of the structure emphasizing a Cl atom appearing in a tetrahedron formed by a Si atom with three additional oxygen atoms. Chlorine blocks the formation of a Si-O bond here forming a free termination. Figure 8 (b) shows another example in the same structure where the Chlorine atom is placed in a ring instead of a Si atom. O-Cl-O triplet is featured here that is clearly defined by the force-field developed by Ohta and Hamaguchi[22]. The glass-member ring structure distribution obtained with different Cl doping amount is shown in Figure 8 (c). This indicates a trend with increasing amount of a nine membered ring, a ten membered ring, an eleven membered ring and a twelve membered ring with increasing Cl concentration. The break-up of certain Si-O bonds by Cl is likely resulting in larger ring sizes than in the absence of Cl atoms. Figure 8 (d) shows a structure obtained from MD simulation adding Fluorine to the SiO_2 system. Five-fold coordination is a viable possibility in Si coordination[24].

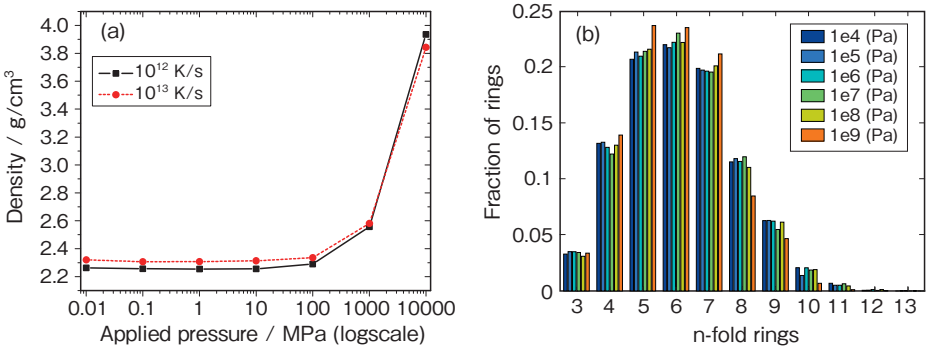

Figure 7 (a) Density changes of the obtained glass structure applying different pressure on the melted state of the drawn fiber (b) The glass-member ring structure distribution of the structure obtained applying different pressures.

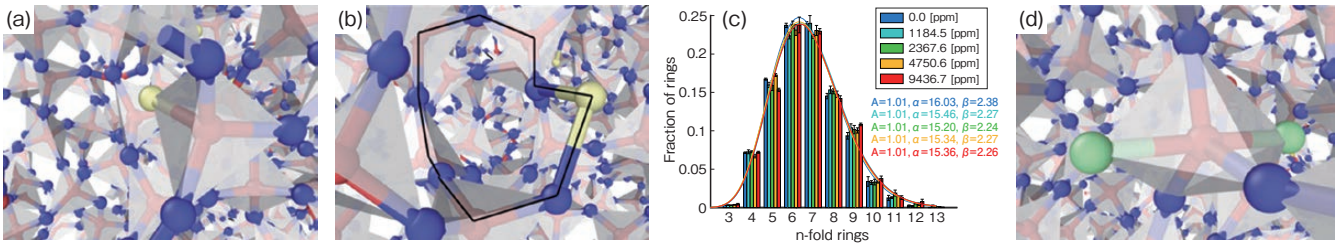

Figure 8 (a) Obtained structure with Cl (yellow) appearing in a tetrahedron formed around a Si (red), (b) Cl is appearing in a silica-four membered ring between two oxygens (blue) (c) The membered ring structure distributions with different Chlorine concentration, (d) Fluorine doped SiO_2 with interesting five-fold coordination of silica.

4. CONCLUSION

We have derived the loss formula for the micro-bending loss in case of two different Gaussian deformations caused by sandpaper particles including the important mechanical properties of the fiber glass and coatings. We compared the experimental and simulation results using three different power spectrum functions after optimizing the simulation parameters in the loss formula given in Equation (6). We calculated the wavelength dependent behavior of two different fibers, and we demonstrated how we can use the developed model to select low micro-bending loss fibers.

We demonstrated MD simulations by the Vashishta, Tersoff and Ohta force-fields to capture the effects of annealing process, pressure effects and the impact of doping on the fiber glass during the drawing process. We found the following statements in connection with glass structure. (1) Low cooling rate is advantageous from the scattering loss point of view. (2) Applied pressure on the melted state of the fiber glass suppresses high number membered rings that also reduces the scattering of light due to local density fluctuations. (3) Cl doping showed increasing nine to eleven membered rings blocking the formation of smaller membered ring structures. This doping effect and its consequences require further analyses.

REFERENCES

1) https://www.furukawa.co.jp/en/release/2018/comm_180330.html
2) K. Mukasa, T. Mihálffy and Z. Várallyay: "Optimizations of thin glass diameter fibers," in Optical Fiber Communication Conference (OFC) 2021, OSA Technical Digest, paper M3C.1.
3) T. Mihálffy, Z. Várallyay, G. Varga and K. Mukasa: "Combined Mechanical-Optical Simulation to Predict Microbending Loss of Single Mode Fibers," 2019 24th OptoElectronics and Communications Conference (OECC) and 2019 International Conference on Photonics in Switching and Computing (PSC), 2019, pp. 1-3, doi: 10.23919/PS.2019.8818048.
4) Z. Várallyay, T. Mihálffy, S. Bilicz, G. Varga, and K. Mukasa: "Microbending Loss Properties of Different Fiber Designs" in Optical Fiber Communication Conference (OFC) 2021, OSA Technical Digest, paper Th1A.49.
5) Z. Várallyay, T. Mihálffy and K. Mukasa: "Comparison of Different Deformation Functions Modeling Micro-bending Loss of Optical Fibers on Sandpaper Test," in Optical Fiber Communication Conference (OFC) 2022, OSA Technical Digest, paper M4E.3.
6) Z. Várallyay, K. Mukasa, B. Csengeri, Zs. Puskás, B. Németh and P. Szelestey: "Silica glass structure simulation for optical fiber application," 2020 Opto-Electronics and Communications Conference (OECC), 2020, pp. 1-3, doi: 10.1109/OECC48412.2020.9273632.
7) D. Marcuse, Theory of Dielectric Optical Waveguides, (Academic Press, second ed. 1991), Chap. 3.
8) W. B. Gardner: "Microbending Loss in Optical Fibers." Bell System Technical Journal, 54, 457–465 (1975).
9) R. Ahmad, W. Ko, K. S. Feder, and P. S. Westbrook: "Measuring the shape of microbends in optical fibers," Optics Express 45, 5189-5192, (2020).
10) R. Olshansky: "Distortion Losses in Cabled Optical Fibers," Applied Optics, 14, 20–21 (1975).
11) P. Sillard: "New fibers for ultra-high capacity transport," Optical Fiber Technology, 17, 495–502 (2011).
12) B. Champagnon, C. Chemarin, E. Duval and R. Le Parc: "Glass structure and light scattering," Journal of Non-Crystalline Solids, vol. 274, pp. 81-86, (2000).
13) X. Bidault, S. Chaussedent, W. Blanc, and D. R. Neuville: "Deformation of silica glass studied by molecular dynamics: Structural origin of the anisotropy and non-Newtonian behavior," Journal of Non-Crystalline Solids, vol. 43, pp. 38–44, (2016).
14) P. Koziatek, J. L. Barrat and D. Rodney: "Short- and medium-range orders in as-quenched and deformed SiO_2 glasses: An atomistic study," Journal of Non-Crystalline Solids, vol. 414, pp. 7–15, (2015).
15) A. E. Geissberger and F. L. Galeener: "Raman studies of vitreous SiO_2 versus fictive temperature," Physical Review B, vol. 28, pp. 3266, (1983).
16) Y. Tamura, H. Sakuma, K. Morita, M. Suzuki, Y. Yamamoto, K. Shimada, Y. Honma, K. Sohma, T. Fujii and T. Hasegawa: "Lowest-ever 0.1419-dB/km loss optical fiber," OFC 2017 conference, paper Th5D.1, 2017.
17) M. Ono, S. Aoyama, M. Fujinami, and S. Ito: "Significant suppression of Rayleigh scattering loss in silica glass formed by the compression of its melted phase," Optics Express, vol. 26, pp. 7942-7948, (2018).
18) Y. Yang, O. Homma, S. Urata, M. Ono and J. C. Mauro: "Topological pruning enables ultra-low Rayleigh scattering in pressure-quenched silica glass," npj Computational Materials vol. 6, pp. 139, (2020).
19) J. Schroeder, R. Mohr, P. B. Macedo and C. J. Montrose: "Rayleigh and Brillouin Scattering in K_2O-SiO_2 Glasses", Journal of The American Ceramic Society, vol. 56, pp. 510-514, (1973).
20) P. Vashishta, R. K. Kalia, J. P. Rino and I. Ebbsjö: "Interaction potential for SiO_2: A molecular dynamics study of structural correlations," Physical Review B, vol. 41, pp. 12197-12209, (1990).
21) J. Tersoff: "New empirical approach for the structure and energy of covalent systems," Physical Review B, vol. 37, pp. 6991-7000, (1988).
22) H. Ohta and S. Hamaguchi: "Classical interatomic potentials for Si-O-F and Si-O-Cl systems," J. Chemical Physics, vol. 115, pp. 6679-6690, (2001).
23) S. Munetoh, T. Motooka, K. Moriguchi and A. Shintani: "Interatomic potential for Si-O systems using Tersoff parameterization," Computational Materials Science Vol. 39, pp. 334-339 (2007).
24) J. R. Rustad, D. A. Yuen, F. J. Spera: "Coordination variability and the structural components of silica glass under high pressures," Chemical Geology vol. 96, pp 421-437 (1992).